research communications

Carbon dioxide capture from air leading to bis[N-(5-methyl-1H-pyrazol-3-yl-κN^2)carbamato-κO]copper(II) tetrahydrate

Valerii Y. Sirenko,[a]* Iryna S. Kuzevanova,[b,c] Oleksandr S. Vynohradov,[a] Dina D. Naumova[a] and Sergiu Shova[d]

[a]Department of Chemistry, Taras Shevchenko National University of Kyiv, Volodymyrska str. 64/13, 01601 Kyiv, Ukraine, [b]Department of General and Inorganic Chemistry, National Technical University of Ukraine "Igor Sikorsky Kyiv Polytechnic Institute", Peremogy Pr. 37, 03056 Kyiv, Ukraine, [c]Innovation Development Center ABN, Pirogov str. 2/37, 01030 Kyiv, Ukraine, and [d]Department of Inorganic polymers, "Petru Poni" Institute of Macromolecular Chemistry, Aleea Gr. Ghica, Voda 41A, 700487 Iasi, Romania. *Correspondence e-mail: valerii_sirenko@knu.ua

A mononuclear square-planar Cu^{II} complex of (5-methyl-1H-pyrazol-3-yl) carbamate, [Cu(C$_5$H$_6$N$_3$O$_2$)$_2$]·4H$_2$O, was synthesized using a one-pot reaction from 5-methyl-3-pyrazolamine and copper(II) acetate in water under ambient conditions. The adsorption of carbon dioxide from air was facilitated by the addition of diethanolamine to the reaction mixture. While diethanolamine is not a component of the final product, it plays a pivotal role in the reaction by creating an alkaline environment, thereby enabling the adsorption of atmospheric carbon dioxide. The central copper(II) atom is in an (N$_2$O$_2$) square-planar coordination environment formed by two N atoms and two O atoms of two equivalent (5-methyl-1H-pyrazol-3-yl)carbamate ligands. Additionally, there are co-crystallized water molecules within the crystal structure of this compound. These co-crystallized water molecules are linked to the Cu^{II} mononuclear complex by O—H$\cdots$O hydrogen bonds. According to Hirshfeld surface analysis, the most frequently observed weak intermolecular interactions are H$\cdots$O/O$\cdots$H (33.6%), H$\cdots$C/C$\cdots$H (11.3%) and H$\cdots$N/N$\cdots$H (9.0%) contacts.

1. Chemical context

Currently, global warming stands out as the most significant environmental concern, leading to climate change and giving rise to a range of effects, including elevated sea levels, prolonged droughts, intensified hurricanes, and a surge in extreme weather occurrences (Ochedi et al., 2021). The primary cause of global warming in recent decades can be attributed to the heightened levels of greenhouse gases in the atmosphere, with particular emphasis on the concentration of CO_2 (Aghaie et al., 2018). Power plants, comprising more than 40% of CO_2 emissions, with coal-fired facilities accounting for 73% of fossil fuel-based power plant emissions (Cannone et al., 2021; Mikkelsen et al., 2010), are a significant contributor to the carbon footprint. Given the widespread use of fossil fuels, particularly coal, there is a strong need to develop effective methods for capturing and mitigating CO_2 emissions from power plant flue gases, to help stabilize the atmospheric CO_2 level (Wang et al., 2017).

Various technologies, including adsorption (Milner et al., 2017), absorption (Conway et al., 2013), membrane separations (Sreedhar et al., 2017), cryogenic distillation (Song et al., 2019), and chemical looping (Kronberger et al., 2004), are currently under research and development for capturing CO_2 from flue-gas streams. One potential strategy for reducing
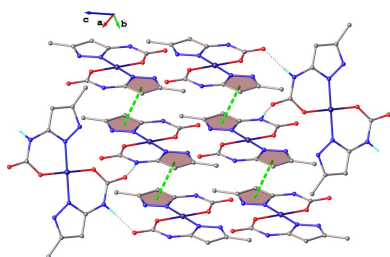
carbon emissions in the future involves the utilization of carbon capture and sequestration (CCS) materials.

The process of CCS entails the specific separation and subsequent storage of CO_2 taken from exhaust gas mixtures, which predominantly consist of N_2, CO_2, H_2O, and O_2, preventing their release into the atmosphere. Following this, the collected CO_2 is transported for either utilization or long-term storage. Amine scrubbing-based chemical capture methods have garnered significant focus and interest (Tang *et al.*, 2005; Mani *et al.*, 2006).

One of the methods for reducing carbon dioxide levels in the environment involves capturing it through the formation of carbamates (Conway *et al.*, 2011; McCann *et al.*, 2009; Zhang *et al.*, 2017). Besides, carbamates can be used as catalysts or useful intermediates in the synthesis of other, more-valuable chemicals (Dell'Amico *et al.*, 2003). Given the necessity of capturing CO_2 to address broader societal needs, in this article we report the synthesis, crystal structure and Hirshfeld surface analysis of a new mononuclear copper(II) complex with (5-methyl-1*H*-pyrazol-3-yl)carbamic acid – [Cu(5-MeHpzCarb)$_2$]·4H$_2$O.
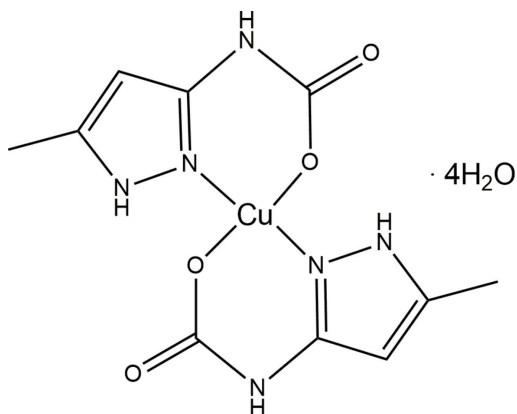
2. Structural commentary

The title compound crystallizes in the monoclinic space group $P2_1/c$, and has a crystal structure built upon neutral mononuclear [Cu(5-MeHpzCarb)$_2$] units (Fig. 1). Co-crystallized water molecules are present in a 1:4 ratio to the complex as interstitial molecules. The asymmetric unit includes one copper site (SOF is 0.5, Wyckoff position 2a), one (5-methyl-1*H*-pyrazol-3-yl)carbamate ligand and two co-crystallized water molecules.

The Cu^{II} ion displays a square-planar coordination environment (N$_2$O$_2$) formed by two nitrogen atoms of pyrazole rings and two oxygen atoms of carboxylate group of (5-methyl-1*H*-pyrazol-3-yl)carbamate ligands. The Cu1—N1 distances are 1.931 (2) Å while the Cu1–O1 distances are shorter and account to 1.9140 (17) Å. The O1–Cu1–O1^i and N1—Cu1—N1^i bond angles are 180°, which is typical for a square-planar arrangement (Fig. 1). At the same time, the N1—Cu1—O1^i and N1—Cu1—O1 bond angles slightly deviate from the ideal value of 90°, which is the result of the formation of the six-membered chelate rings. Selected bond

Table 1
Selected bond lengths and bond angles (Å, °).

| Cu1—O1	1.9140 (17)	Cu1—N1	1.931 (2)
N1^i—Cu1—N1	180.0	O1—Cu1—N1^i	91.08 (8)
O1—Cu1—N1	88.92 (8)	N2—N1—Cu1	126.70 (16)

Symmetry codes: (i) $-x, -y, -z$

lengths and bond angles are given in Table 1. The Cu1 atom lies within the plane defined by N1—O1—N1^i—O1^i. Additionally, the Cu atom lies within the planes of the aromatic rings, whereas O1 and O1^i are slightly above the plane, with an O1(O1^i)-to-plane distance of 0.182 (3) Å.

In the crystal structure, monomeric [Cu(5-MeHpzCarb)$_2$] units form layers with Cu1 centres lying in the *ab* plane. The plane-normal-to-plane-normal angle between the horizontal N1—O1—N1^i—O1^i planes of two adjacent layers is 74.762 (2)°.

3. Supramolecular features

All the components of the structure are associated *via* intermolecular O—H···O and N—H···O hydrogen bonds, as well as weak C—H···O contacts (Figs. 2, 3). π–π contacts are also observed between neutral [Cu(5-MeHpzCarb)$_2$] molecular complexes (Fig. 2). The co-crystallized water molecules are interleaved with the supramolecular layers of the neutral [Cu(5-MeHpzCarb)$_2$] complexes along the *c*-axis. The O4 water molecule participates in four hydrogen bonds, two where it acts as a donor (O4—H4*E*···O2^{ii} and O4—H4*D*···O3^i, see Table 2 for details), and two as acceptor
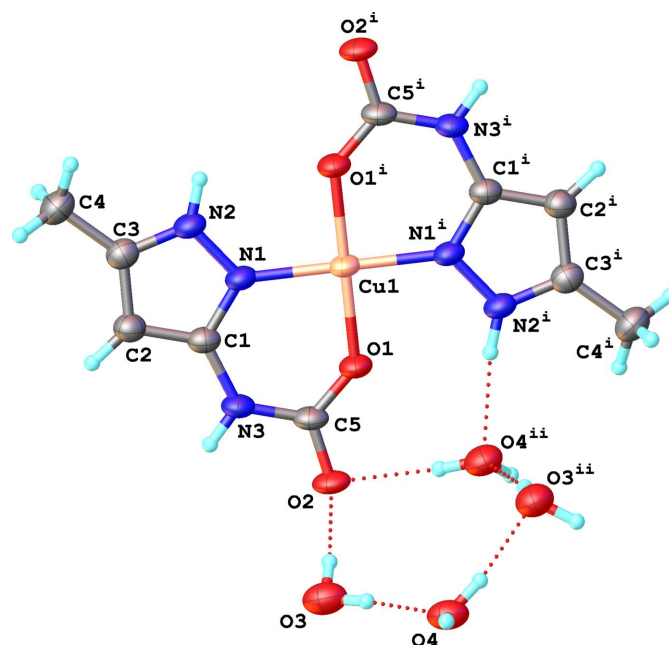
Figure 1
Representation of the [Cu(5-MeHpzCarb)$_2$] complex and co-crystallized water molecules, showing the atom-labelling scheme and displacement ellipsoids drawn at the 50% probability level. H atoms are shown as small spheres of arbitrary radii. Symmetry codes: (i) $-x, -y, -z$; (ii) $1 - x$, $-\frac{1}{2} + y$, $\frac{1}{2} - z$.

Table 2
Hydrogen-bond geometry (Å, °).

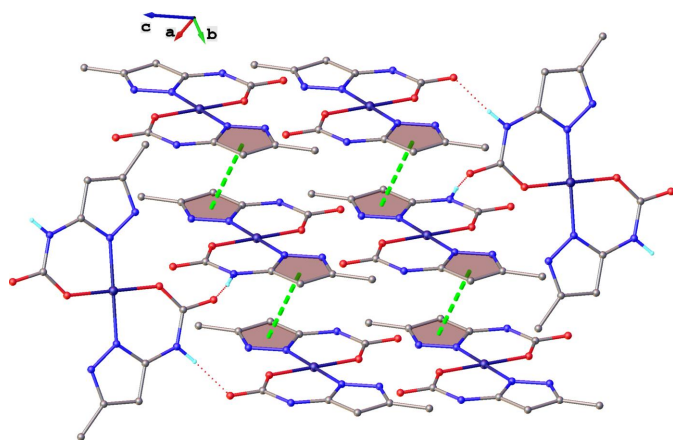| $D—H\cdots A$	$D—H$	$H\cdots A$	$D\cdots A$	$D—H\cdots A$
O4—H4$D$$\cdots$O3^{i}	0.87	1.80	2.664 (3)	171
O4—H4$E$$\cdots$O1^{ii}	0.87	2.44	2.930 (3)	116
O4—H4$E$$\cdots$O2^{ii}	0.87	2.02	2.873 (3)	167
N2—H2$\cdots$O4^{iii}	0.88	1.99	2.863 (3)	169
N3—H3$\cdots$O2^{iv}	0.88	2.02	2.889 (3)	169
O3—H3$A$$\cdots$O2	0.87	1.89	2.756 (3)	176
O3—H3$B$$\cdots$O4	0.87	1.92	2.783 (3)	169
C2—H2$A$$\cdots$O3^{iv}	0.95	2.43	3.340 (4)	159

Symmetry codes: (i) $-x + 1, y - \frac{1}{2}, -z + \frac{1}{2}$; (ii) $-x + 1, y + \frac{1}{2}, -z + \frac{1}{2}$; (iii) $x - 1, -y + \frac{1}{2}, z - \frac{1}{2}$; (iv) $-x, y + \frac{1}{2}, -z + \frac{1}{2}$.

(O3—H3$B$$\cdots$O4 and N2—H2$\cdots$O4^{iii}, see Table 2 for details). At the same time, the O3 water molecule participates in three hydrogen bonds, two where it acts as a donor (O3—H3$A$$\cdots$O2 and O3—H3$B$$\cdots$O4, see Table 2 for details) and one as acceptor (O4—H4$D$$\cdots$O3^{i}, see Table 2 for details). In addition, the O3 water molecule participates in a weak C2—H2$A$$\cdots$O3^{iv} contact with a C2$\cdots$O3 distance of 3.340 (4) Å. According to this, the co-crystallized water molecules play an important role in providing cohesion between the neutral [Cu(5-MeHpzCarb)$_2$] molecular complexes. Geometric parameters for intermolecular hydrogen bonds are given in Table 2.
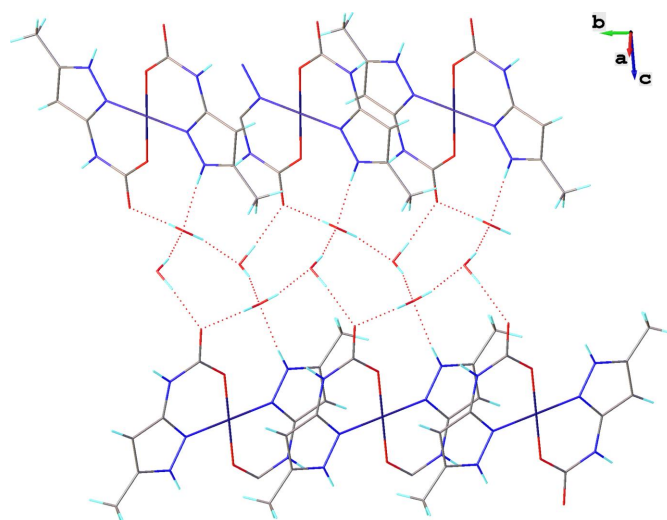
Interestingly, four water molecules and the carboxyl group form a five-membered supramolecular ring (Fig. 3). In addition, π–π interactions are observed between the [Cu(5-MeHpzCarb)$_2$] neutral complexes. The plane-to-plane distance for these π–π contacts is 3.324 (3) Å with the plane-to-plane shift being 1.498 (5) Å. It is also worth noting very weak C—H$\cdots$$\pi$ contacts between two contiguous [Cu(5-MeHpzCarb)$_2$] units with a carbon-atom-to-plane distance of 3.586 (4) Å.

4. Hirshfeld surface analysis

The Hirshfeld surface analysis was performed and the associated two-dimensional fingerprint plots were generated using
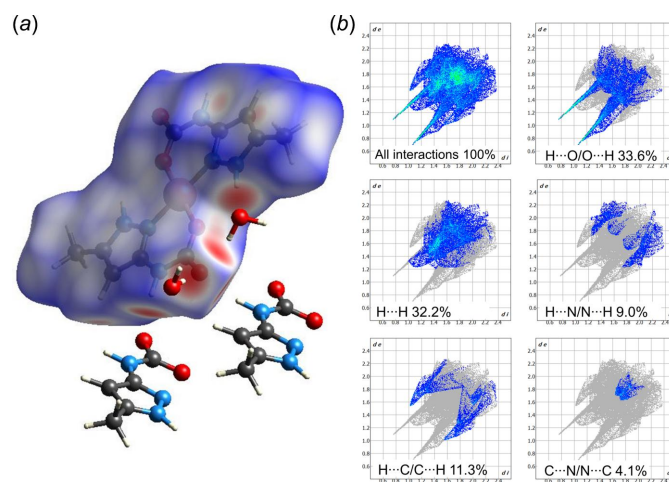

Figure 3
Partial crystal packing of [Cu(5-MeHpzCarb)$_2$]·4H$_2$O showing the five-membered supramolecular ring formed by four water molecules and the carboxyl group of the (5-methyl-1H-pyrazol-3-yl)carbamate ligand.

Crystal Explorer 21.5 software (Spackman *et al.*, 2021), with standard resolution of the three-dimensional d_{norm} surfaces plotted over a fixed colour scale of −0.6468 (red) to 1.1041 (blue) a.u. There are eight red spots on the d_{norm} surface (Fig. 4a). Visualizations were performed using a red–white–blue colour scheme, where red highlights shorter contacts, white is used for contacts around vdW separation, and blue depicts longer contacts. The red spots on the 3D d_{norm} Hirshfeld surfaces indicate the direction and strength of the intermolecular E—H$\cdots$O hydrogen bonds (where E = N, O), as well as weak C—H$\cdots$O and C—H$\cdots$$\pi$ contacts. The overall two-dimensional fingerprint plots for the selected interactions are shown in Fig. 4b.

The most significant contributions to the overall crystal packing are from H$\cdots$H (32.2%), H$\cdots$O/O$\cdots$H (33.6%),

Figure 2
Partial crystal packing of [Cu(5-MeHpzCarb)$_2$]·4H$_2$O showing intermolecular π–π and N—H$\cdots$O contacts as green and red dashed lines, respectively.

Figure 4
(a) Hirshfeld surface representations with the function d_{norm} plotted onto the surface for the different interactions; (b) two-dimensional fingerprint plots, showing the contributions of different types of interactions.

H⋯C/C⋯H (11.3%), H⋯N/N⋯H (9.0%) and C⋯N/ N⋯C (4.1%) interactions. The H⋯O/O⋯H contacts form a pair of spikes on the sides of the corresponding two-dimensional plot, which are indicative of strong intermolecular interactions between atoms. At the same time, the H⋯N/ N⋯H and H⋯C/C⋯H contacts form less pronounced spikes, indicating that these interactions are weaker.

5. Database survey

A search of the Cambridge Structure Database (CSD version 5.44, last update June 2023; Groom *et al.*, 2016) revealed that the structure has never been published before. 51 structures for the $Cu(pyrazole)_2(CO_2)_2$ moiety [four-coordinated copper atom with an N_2O_2 coordination environment] were found. Most similar to the title compound, complexes forming a four-coordinated N_2O_2 coordination environment, are *trans*-bis-(3,5-dimethylpyrazole)bis(pivalato)copper(II) (DEFSAJ; Zhou *et al.*, 2006), bis(1*H*-indazole-3-carboxylato)copper(II) (ETOVUH; Qin *et al.*, 2017), *trans*-bis(4-nitrobenzoato-*O*) bis(3,5-dimethylpyrazole-*N*)copper(II) (KOKGIB; Sarma & Baruah, 2008) and bis(dimethylammonium) bis(μ_2-3,5-dicarboxylatopyrazolato)dicopper(II) (ALERIU; Demir *et al.*, 2016).

6. Synthesis and crystallization

5-Methyl-3-pyrazolamine (0.015 g, 1.54×10^{-4} mol), copper(II) acetate (0.28 g, 1.54×10^{-4} mol) and diethanolamine (0.032 g, 3.08×10^{-4} mol) were mixed together, and dissolved in water. After 3 days, clear, light-violet crystals were collected by filtration, dried for less than a minute, and then placed under crystallographic oil for further measurements.

7. Refinement

Crystal data, data collection and structure refinement details are summarized in Table 3. The H atoms of $N_{(p, c)}$—H, C_p—H and O_w—H groups (p = pyrazole, c = carbamide, w = water) were positioned geometrically and refined as riding atoms, with C—H = 0.95 Å and $U_{iso}(H) = 1.2U_{eq}(C)$ for C_p—H groups, N—H = 0.88 Å and $U_{iso}(H) = 1.2U_{eq}(N)$ for $N_{(p, c)}$—H groups and O—H = 0.87 Å and $U_{iso}(H) = 1.5U_{eq}(O)$ for O_w—H groups. Methyl H atoms were positioned geometrically and were allowed to ride on C atoms and rotate around the C—C bond, with C—H = 0.98 Å and $U_{iso}(H) = 1.5U_{eq}(C)$ for the CH_3 groups.

Table 3
Experimental details.

Crystal data	
Chemical formula	$[Cu(C_5H_6N_3O_2)_2]\cdot4H_2O$
M_r	415.86
Crystal system, space group	Monoclinic, $P2_1/c$
Temperature (K)	200
a, b, c (Å)	8.4623 (2), 5.64870 (16), 17.4536 (4)
β (°)	98.786 (2)
V (Å^3)	824.51 (4)
Z	2
Radiation type	Cu $K\alpha$
μ (mm^{-1})	2.39
Crystal size (mm)	$0.15 \times 0.15 \times 0.15$
Data collection	
Diffractometer	XtaLAB Synergy, Dualflex, HyPix
Absorption correction	Multi-scan (*CrysAlis PRO*; Rigaku OD, 2023)
T_{min}, T_{max}	0.638, 1.000
No. of measured, independent and observed [$I > 2\sigma(I)$] reflections	5223, 1634, 1401
R_{int}	0.042
$(\sin\theta/\lambda)_{max}$ (Å^{-1})	0.631
Refinement	
$R[F^2 > 2\sigma(F^2)], wR(F^2), S$	0.041, 0.118, 1.05
No. of reflections	1634
No. of parameters	116
No. of restraints	2
H-atom treatment	H-atom parameters constrained
$\Delta\rho_{max}, \Delta\rho_{min}$ (e Å^{-3})	0.45, −0.57

Computer programs: *CrysAlis PRO* (Rigaku OD, 2023), *SHELXT2018/2* (Sheldrick, 2015*b*), *SHELXL2018/3* (Sheldrick, 2015*a*) and *OLEX2* (Dolomanov *et al.*, 2009).

References

Aghaie, M., Rezaei, N. & Zendehboudi, S. (2018). *Renew. Sustain. Energy Rev.* **96**, 502–525.
Cannone, S. F., Lanzini, A. & Santarelli, M. (2021). *Energies* **14**, 387.
Conway, W., Fernandes, D., Beyad, Y., Burns, R., Lawrance, G., Puxty, G. & Maeder, M. (2013). *J. Phys. Chem. A*, **117**, 806–813.
Conway, W., Wang, X., Fernandes, D., Burns, R., Lawrance, G., Puxty, G. & Maeder, M. (2011). *J. Phys. Chem. A*, **115**, 14340–14349.
Dell'Amico, D. B., Calderazzo, F., Labella, L., Marchetti, F. & Pampaloni, G. (2003). *Chem. Rev.* **103**, 3857–3898.
Demir, S., Çepni, H. M., Hołyńska, M. & Kavanoz, M. (2016). *Z. Naturforsch.* **71**, 305–310.
Dolomanov, O. V., Bourhis, L. J., Gildea, R. J., Howard, J. A. K. & Puschmann, H. (2009). *J. Appl. Cryst.* **42**, 339–341.
Groom, C. R., Bruno, I. J., Lightfoot, M. P. & Ward, S. C. (2016). *Acta Cryst.* B**72**, 171–179.
Kronberger, B., Johansson, E., Löffler, G., Mattisson, T., Lyngfelt, A. & Hofbauer, H. (2004). *Chem. Eng. Technol.* **27**, 1318–1326.
Mani, F., Peruzzini, M. & Stoppioni, P. (2006). *Green Chem.* **8**, 995–1000.
McCann, N., Phan, D., Wang, X., Conway, W., Burns, R., Attalla, M., Puxty, G. & Maeder, M. (2009). *J. Phys. Chem. A*, **113**, 5022–5029.
Mikkelsen, M., Jørgensen, M. & Krebs, F. C. (2010). *Energy Environ. Sci.* **3**, 43–81.
Milner, P. J., Siegelman, R. L., Forse, A. C., Gonzalez, M. I., Runčevski, T., Martell, J. D., Reimer, J. A. & Long, J. R. (2017). *J. Am. Chem. Soc.* **139**, 13541–13553.
Ochedi, F. O., Yu, J., Yu, H., Liu, Y. & Hussain, A. (2021). *Environ. Chem. Lett.* **19**, 77–109.
Qin, G.-F., Qin, Q.-Y., Long, B.-F., Wei, D.-P., Xu, Y.-H., Bao, S.-J. & Yin, X.-H. (2017). *J. Iran. Chem. Soc.* **14**, 1227–1234.

Rigaku OD (2023). *CrysAlis PRO*. Rigaku Oxford Diffraction, Yarnton, England.

Sarma, R. & Baruah, J. B. (2008). *J. Coord. Chem.* **61**, 3329–3335.

Sheldrick, G. M. (2015*a*). *Acta Cryst.* A**71**, 3–8.

Sheldrick, G. M. (2015*b*). *Acta Cryst.* C**71**, 3–8.

Song, C., Liu, Q., Deng, S., Li, H. & Kitamura, Y. (2019). *Renew. Sustain. Energy Rev.* **101**, 265–278.

Spackman, P. R., Turner, M. J., McKinnon, J. J., Wolff, S. K., Grimwood, D. J., Jayatilaka, D. & Spackman, M. A. (2021). *J. Appl. Cryst.* **54**, 1006–1011.

Sreedhar, I., Vaidhiswaran, R., Kamani, B. M. & Venugopal, A. (2017). *Renew. Sustain. Energy Rev.* **68**, 659–684.

Tang, Y., Kassel, W. S., Zakharov, L. N., Rheingold, A. L. & Kemp, R. A. (2005). *Inorg. Chem.* **44**, 359–364.

Wang, Y., Zhao, L., Otto, A., Robinius, M. & Stolten, D. (2017). *Energy Procedia*, **114**, 650–665.

Zhang, R., Yang, Q., Liang, Z., Puxty, G., Mulder, R. J., Cosgriff, J. E., Yu, H., Yang, X. & Xue, Y. (2017). *Energy Fuels*, **31**, 11099–11108.

Zhou, J.-H., Liu, Z., Li, Y.-Z., Song, Y., Chen, X.-T. & You, X.-Z. (2006). *J. Coord. Chem.* **59**, 147–156.

supporting information

Carbon dioxide capture from air leading to bis[*N*-(5-methyl-1*H*-pyrazol-3-yl-*κN²*)carbamato-*κO*]copper(II) tetrahydrate

Valerii Y. Sirenko, Iryna S. Kuzevanova, Oleksandr S. Vynohradov, Dina D. Naumova and Sergiu Shova

Computing details

Data collection: *CrysAlis PRO* 1.171.42.93a (Rigaku OD, 2023); cell refinement: *CrysAlis PRO* 1.171.42.93a (Rigaku OD, 2023); data reduction: *CrysAlis PRO* 1.171.42.93a (Rigaku OD, 2023); program(s) used to solve structure: *SHELXT2018/2* (Sheldrick, 2015b); program(s) used to refine structure: *SHELXL2018/3* (Sheldrick, 2015a); molecular graphics: Olex2 1.5 (Dolomanov *et al.*, 2009); software used to prepare material for publication: Olex2 1.5 (Dolomanov *et al.*, 2009).

Bis[*N*-(5-methyl-1*H*-pyrazol-3-yl-*κN²*)carbamato-*κO*]copper(II) tetrahydrate

Crystal data

$[Cu(C_5H_6N_3O_2)_2] \cdot 4H_2O$	$F(000) = 430$
$M_r = 415.86$	$D_x = 1.675$ Mg m^{-3}
Monoclinic, $P2_1/c$	Cu $K\alpha$ radiation, $\lambda = 1.54184$ Å
$a = 8.4623$ (2) Å	Cell parameters from 2285 reflections
$b = 5.64870$ (16) Å	$\theta = 5.1$–$72.3°$
$c = 17.4536$ (4) Å	$\mu = 2.39$ mm^{-1}
$\beta = 98.786$ (2)°	$T = 200$ K
$V = 824.51$ (4) Å^3	Block, clear light violet
$Z = 2$	$0.15 \times 0.15 \times 0.15$ mm

Data collection

XtaLAB Synergy, Dualflex, HyPix diffractometer	1634 independent reflections
	1401 reflections with $I > 2\sigma(I)$
Detector resolution: 10.0000 pixels mm^{-1}	$R_{int} = 0.042$
ω scans	$\theta_{max} = 76.8°$, $\theta_{min} = 5.1°$
Absorption correction: multi-scan (CrysAlisPro; Rigaku OD, 2023)	$h = -10 \rightarrow 10$
	$k = -6 \rightarrow 4$
$T_{min} = 0.638$, $T_{max} = 1.000$	$l = -16 \rightarrow 22$
5223 measured reflections	

Refinement

Refinement on F^2	116 parameters
Least-squares matrix: full	2 restraints
$R[F^2 > 2\sigma(F^2)] = 0.041$	Primary atom site location: dual
$wR(F^2) = 0.118$	Hydrogen site location: mixed
$S = 1.05$	H-atom parameters constrained
1634 reflections	

$w = 1/[\sigma^2(F_o^2) + (0.0636P)^2 + 0.4306P]$
　　where $P = (F_o^2 + 2F_c^2)/3$
$(\Delta/\sigma)_{max} < 0.001$

$\Delta\rho_{max} = 0.45$ e Å^{-3}
$\Delta\rho_{min} = -0.57$ e Å^{-3}

Special details

Geometry. All esds (except the esd in the dihedral angle between two l.s. planes) are estimated using the full covariance matrix. The cell esds are taken into account individually in the estimation of esds in distances, angles and torsion angles; correlations between esds in cell parameters are only used when they are defined by crystal symmetry. An approximate (isotropic) treatment of cell esds is used for estimating esds involving l.s. planes.

Fractional atomic coordinates and isotropic or equivalent isotropic displacement parameters (Å²)

	x	*y*	*z*	U_{iso}*/U_{eq}
Cu1	0.000000	0.000000	0.000000	0.0327 (2)
O4	0.6601 (3)	0.2829 (4)	0.29517 (11)	0.0518 (6)
H4D	0.663197	0.160498	0.265176	0.078*
H4E	0.733747	0.377068	0.282986	0.078*
N2	−0.2338 (3)	0.3798 (4)	−0.05018 (12)	0.0354 (5)
H2	−0.253149	0.326001	−0.098018	0.042*
N1	−0.1348 (2)	0.2716 (4)	0.00870 (11)	0.0331 (5)
N3	−0.0507 (3)	0.3550 (4)	0.14235 (11)	0.0362 (5)
H3	−0.059104	0.455034	0.180169	0.043*
O3	0.3513 (3)	0.4313 (5)	0.30719 (12)	0.0567 (6)
H3A	0.280457	0.334940	0.282998	0.085*
H3B	0.442727	0.365820	0.303128	0.085*
C1	−0.1376 (3)	0.4090 (5)	0.07052 (14)	0.0327 (5)
C2	−0.2365 (3)	0.6047 (5)	0.05156 (15)	0.0368 (6)
H2A	−0.257394	0.729896	0.084961	0.044*
C4	−0.4112 (3)	0.7265 (6)	−0.07931 (17)	0.0455 (7)
H4A	−0.388986	0.707721	−0.132463	0.068*
H4B	−0.398069	0.893005	−0.063909	0.068*
H4C	−0.521048	0.676241	−0.076675	0.068*
C3	−0.2977 (3)	0.5781 (5)	−0.02590 (15)	0.0360 (6)
C5	0.0462 (3)	0.1642 (5)	0.16088 (13)	0.0339 (6)
O1	0.0677 (2)	0.0130 (3)	0.10968 (10)	0.0391 (5)
O2	0.1152 (2)	0.1456 (4)	0.22973 (9)	0.0400 (5)

Atomic displacement parameters (Å²)

	U^{11}	U^{22}	U^{33}	U^{12}	U^{13}	U^{23}
Cu1	0.0378 (3)	0.0405 (4)	0.0182 (3)	0.0035 (2)	−0.0012 (2)	−0.0008 (2)
O4	0.0577 (12)	0.0586 (14)	0.0355 (10)	−0.0059 (11)	−0.0042 (9)	−0.0031 (9)
N2	0.0403 (11)	0.0409 (13)	0.0228 (10)	0.0015 (10)	−0.0020 (8)	0.0030 (9)
N1	0.0363 (11)	0.0417 (12)	0.0200 (9)	0.0032 (9)	−0.0003 (8)	0.0016 (9)
N3	0.0442 (12)	0.0438 (13)	0.0196 (9)	0.0015 (10)	0.0016 (8)	−0.0031 (9)
O3	0.0618 (14)	0.0628 (14)	0.0418 (12)	−0.0098 (12)	−0.0036 (10)	0.0008 (11)
C1	0.0341 (12)	0.0392 (14)	0.0245 (11)	−0.0040 (11)	0.0036 (9)	−0.0001 (11)
C2	0.0393 (13)	0.0412 (15)	0.0296 (12)	0.0004 (12)	0.0046 (10)	−0.0009 (11)
C4	0.0419 (14)	0.0491 (18)	0.0435 (15)	0.0032 (13)	−0.0004 (12)	0.0085 (13)

C3	0.0352 (12)	0.0391 (14)	0.0336 (13)	−0.0027 (11)	0.0048 (10)	0.0041 (12)
C5	0.0409 (13)	0.0417 (14)	0.0187 (11)	−0.0064 (12)	0.0031 (9)	0.0000 (10)
O1	0.0478 (11)	0.0465 (12)	0.0205 (9)	0.0065 (8)	−0.0028 (8)	−0.0009 (7)
O2	0.0491 (10)	0.0501 (11)	0.0183 (8)	−0.0039 (9)	−0.0026 (7)	0.0022 (8)

Geometric parameters (Å, º)

Cu1—N1	1.931 (2)	N3—C5	1.363 (4)
Cu1—N1^i	1.931 (2)	O3—H3A	0.8697
Cu1—O1	1.9140 (17)	O3—H3B	0.8700
Cu1—O1^i	1.9140 (17)	C1—C2	1.396 (4)
O4—H4D	0.8701	C2—H2A	0.9500
O4—H4E	0.8698	C2—C3	1.380 (4)
N2—H2	0.8800	C4—H4A	0.9800
N2—N1	1.367 (3)	C4—H4B	0.9800
N2—C3	1.341 (4)	C4—H4C	0.9800
N1—C1	1.333 (3)	C4—C3	1.490 (4)
N3—H3	0.8800	C5—O1	1.269 (3)
N3—C1	1.387 (3)	C5—O2	1.258 (3)
N1^i—Cu1—N1	180.0	N1—C1—C2	110.7 (2)
O1^i—Cu1—N1^i	88.92 (8)	N3—C1—C2	127.2 (2)
O1^i—Cu1—N1	91.08 (8)	C1—C2—H2A	127.2
O1—Cu1—N1	88.92 (8)	C3—C2—C1	105.5 (2)
O1—Cu1—N1^i	91.08 (8)	C3—C2—H2A	127.2
O1—Cu1—O1^i	180.0	H4A—C4—H4B	109.5
H4D—O4—H4E	104.5	H4A—C4—H4C	109.5
N1—N2—H2	124.3	H4B—C4—H4C	109.5
C3—N2—H2	124.3	C3—C4—H4A	109.5
C3—N2—N1	111.5 (2)	C3—C4—H4B	109.5
N2—N1—Cu1	126.70 (16)	C3—C4—H4C	109.5
C1—N1—Cu1	127.60 (17)	N2—C3—C2	107.0 (2)
C1—N1—N2	105.3 (2)	N2—C3—C4	121.7 (2)
C1—N3—H3	116.4	C2—C3—C4	131.4 (3)
C5—N3—H3	116.4	O1—C5—N3	120.7 (2)
C5—N3—C1	127.2 (2)	O2—C5—N3	117.9 (2)
H3A—O3—H3B	104.5	O2—C5—O1	121.4 (3)
N1—C1—N3	122.1 (2)	C5—O1—Cu1	132.59 (17)
Cu1—N1—C1—N3	−7.3 (4)	C1—N3—C5—O1	1.3 (4)
Cu1—N1—C1—C2	172.53 (18)	C1—N3—C5—O2	−179.9 (2)
N2—N1—C1—N3	179.7 (2)	C1—C2—C3—N2	−1.3 (3)
N2—N1—C1—C2	−0.4 (3)	C1—C2—C3—C4	179.3 (3)
N1—N2—C3—C2	1.1 (3)	C3—N2—N1—Cu1	−173.46 (18)
N1—N2—C3—C4	−179.4 (2)	C3—N2—N1—C1	−0.5 (3)
N1—C1—C2—C3	1.1 (3)	C5—N3—C1—N1	0.0 (4)

N3—C1—C2—C3	−179.1 (3)	C5—N3—C1—C2	−179.9 (3)
N3—C5—O1—Cu1	5.3 (4)	O2—C5—O1—Cu1	−173.44 (18)

Symmetry code: (i) −*x*, −*y*, −*z*.

Hydrogen-bond geometry (Å, º)

D—H···*A*	*D*—H	H···*A*	*D*···*A*	*D*—H···*A*
O4—H4*D*···O3[ii]	0.87	1.80	2.664 (3)	171
O4—H4*E*···O1[iii]	0.87	2.44	2.930 (3)	116
O4—H4*E*···O2[iii]	0.87	2.02	2.873 (3)	167
N2—H2···O4[iv]	0.88	1.99	2.863 (3)	169
N3—H3···O2[v]	0.88	2.02	2.889 (3)	169
O3—H3*A*···O2	0.87	1.89	2.756 (3)	176
O3—H3*B*···O4	0.87	1.92	2.783 (3)	169
C2—H2*A*···O3[v]	0.95	2.43	3.340 (4)	159

Symmetry codes: (ii) −*x*+1, *y*−1/2, −*z*+1/2; (iii) −*x*+1, *y*+1/2, −*z*+1/2; (iv) *x*−1, −*y*+1/2, *z*−1/2; (v) −*x*, *y*+1/2, −*z*+1/2.